

Large Area Planar Photocathode for MCP-based Photodetectors

Junqi Xie^{a,*}, Klaus Attenkofer^{a,1}, Marcel Demarteau^a, Alexander Paramonov^a, Anatoly Ronzhin^{b,†}, Robert Wagner^a, and Zikri Yusof^{a,2}

^aArgonne National Laboratory, 9700 S Cass Ave., Lemont, IL, 60439 USA

^bFermi National Accelerator Laboratory, PO Box 500, Batavia, IL, 60510 USA

*Corresponding author, email: jxie@anl.gov (J. Xie)

¹Current address: Brookhaven National Laboratory, Upton, NY, 11973 USA

²Current address: Illinois Institute of Technology, Chicago, IL, 60616 USA

[†]Deceased

ABSTRACT

We report on the principle, design, fabrication, and characterization of a large-area planar bialkali photocathode. Sequential photocathode growth process was investigated, and the growth parameters, especially the initial antimony layer thickness, were optimized. The source arrangement and configuration were also simulated and the preferred configuration was chosen for numerical and experimental studies. Photocathode with average QE of 18% and activation area of ~ 40 square inches was experimentally demonstrated, making it a candidate for MCP-based photodetector applications. Further improvements were also discussed to enhance the uniformity and QE value of the photocathodes.

Keywords: *Photomultiplier tube, Microchannel plate, Photocathode, Bialkali antimonide, Large-area planar photodetector*

1. Introduction

Photomultiplier tubes (PMTs) are versatile and sensitive light detectors in the ultraviolet, visible, and near infrared region, and have been extensively used in medical diagnostics, industrial applications and scientific

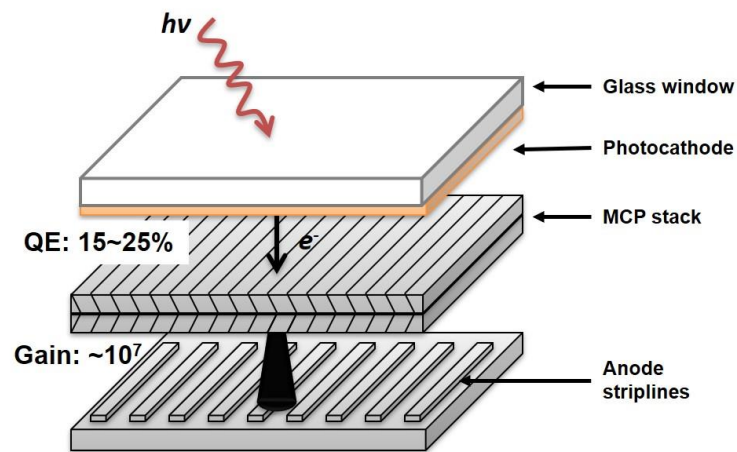
26 research projects. These devices have the ability to resolve single photoelectrons with excellent time
27 resolution [1]. In large neutrino detectors, such as the Super-Kamiokande [2] and Hyper-Kamiokande [3]
28 in Japan, the Jiangmen Underground Neutrino Observatory (JUNO) experiment [4] in China, the original
29 planned Long Baseline Neutrino Experiment (LBNE) [5] and the Accelerator Neutrino Neutron Interaction
30 Experiment (ANNIE) [6] in US, tens of thousands of large area PMTs are currently in use or planned to
31 detect the scintillation or Cerenkov radiation. High-gain, large-area, and cheap planar photodetector would
32 dramatically increase the area coverage, improve the measurement accuracy, and reduce the experimental
33 cost.

34

35 Recent advances in micro-channel plate (MCP) technology [7] and high-speed electronics [8] have provided
36 great opportunities for MCP-based planar photodetectors. MCP based photodetectors are an evolution from
37 the principle of traditional PMTs by replacing the conventional discrete dynodes with MCPs, leading itself
38 to the fast-timing low light level photon counting region. With its micron level pore size for electron
39 amplification, the MCP-based photodetector provides both picosecond timing resolution and sub-mm
40 spatial resolution at the same time. Figure 1 shows the conceptual schematic of an MCP-based large-area
41 picosecond photodetector (LAPPDTM) recently developed and commercialized by the LAPPD collaboration
42 [9]. The main advantage of LAPPD photodetector is the usage of large area, low-cost microchannel plates
43 developed by Argonne National Laboratory and Incom Inc. The new MCP fabrication process relies on two
44 breakthroughs: the glass capillary array technique and the atomic layer deposition. These processes
45 eliminate the soft lead core glass, etching and firing processes in traditional MCP functionalization process,
46 making it possible to fabricate MCPs with an area as large as $20 \times 20 \text{ cm}^2$ at a dramatically reduced cost.
47 The LAPPD photodetector assembly is a rather compact design with minimum detector thickness to ensure
48 the shortest electron travel distance for ps fast timing. Incoming incident photons strike the photocathode
49 and generate free photoelectrons, which produce an avalanche of secondary electrons in MCPs, and the
50 electrons are eventually captured onto the anode. As an essential component of the LAPPDTM photodetector,
51 the photocathode determines many of the MCP-photodetector features including the quantum efficiency

52 (QE), sensitivity, life time, noise behavior, as well as manufacture process, working condition and cost.
53 Large area photocathodes with good spatial uniformity, QE and low noise level are critical to the
54 performance of the large area planar photodetectors.

55
56 In this article, we report the development of bi-alkali antimonide photocathodes at Argonne National
57 Laboratory. Photocathodes in small PMTs were produced through sequential diffusion process and the
58 recipe was transferred to a custom designed glass vessel for large area planar photocathode deposition.



59
60 Figure 1. Conceptual schematic of the LAPPD detector, the photodetector area can be as large as 20×20
61 cm^2 . The photocathode is coated on the inner surface of the top glass window, shown in orange color (online).
62 Note that the dimensions are not scaled.

64 2. Bi-alkali photocathode in small PMT tubes

65 Conventional PMT tubes consist of an alkali photocathode, collection dynode, electron dynodes and an
66 anode. To make the fabrication process easier, the dynodes and anode as well as the photocathode
67 evaporation sources are usually integrated in a pre-made PMT glass tube. Since the alkali photocathodes
68 are air and moisture sensitive, the photocathode deposition is always the last step before vacuum sealing.
69 These integrations make it convenient for the photocathode deposition and vacuum sealing, but occupied
70 large volume of the PMT tube at the end.

71

72 As a starting point to gain expertise in photocathode deposition, we acquired a commercial PMT fabrication
73 facility from Photonis USA Inc. Small photocathodes in vacuum tubes with 1-inch diameter were fabricated
74 using the in-tube photocathode evaporation process. These 1-inch tubes were used to gain photocathode
75 deposition experience and receipt optimization. Sequential diffusion process [10], where antimony and
76 alkali metals are evaporated in sequence, was adopted in our photocathode fabrication.

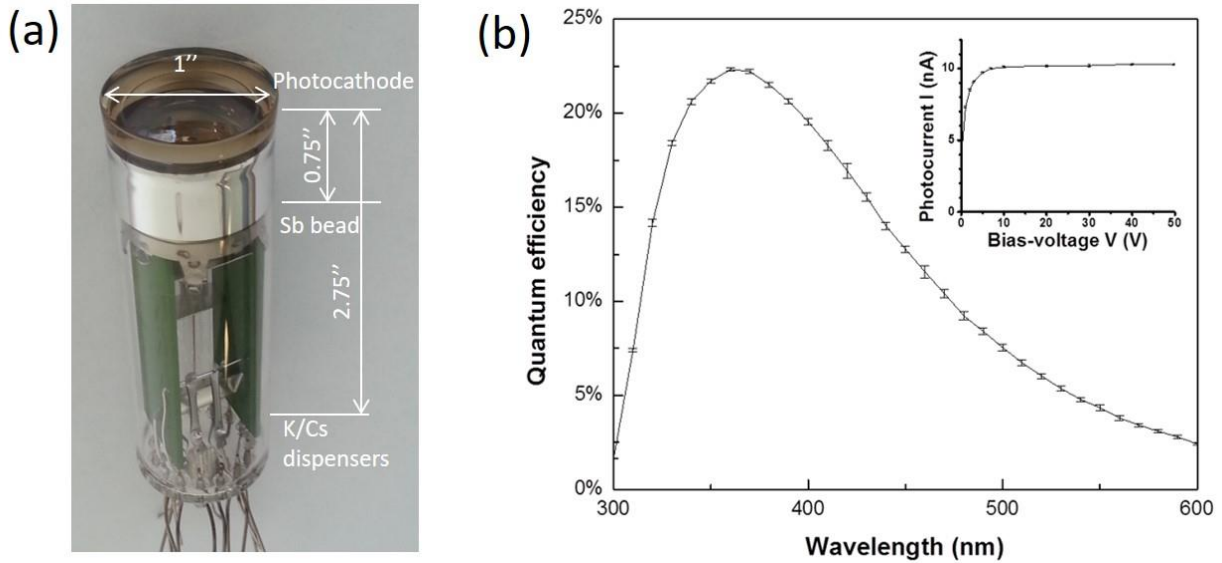
77

78 Prior to the photocathode fabrication, the glass tube was baked at 350 °C under high vacuum overnight to
79 reduce contamination, reaching a base pressure of around 10^{-8} Torr. A thin layer of Sb was first deposited
80 and then oxidized in oxygen plasma, forming antimony oxide as antireflection layer to reduce incoming
81 light reflection. Following this, Sb, K and Cs were then sequentially thermal-evaporated to synthesize
82 bialkali (K-Cs-Sb) photocathode. Antimony/platinum (Sb/Pt) alloy bead (Photonis USA Inc., USA),
83 potassium (K) dispenser and cesium (Cs) dispenser (SAES Getters S.p.A., Italy) were used here as
84 evaporation sources. The diffusion process was controlled by monitoring the photo-current. Figure 2(a)
85 shows a vacuum sealed PMT tube with photocathode on the inner side of the top glass. Dynodes were not
86 integrated in the PMT tube for sole photocathode study and the evaporation sources were sealed in the tube
87 permanently after deposition.

88

89 Electrical and optical properties of the grown photocathodes were characterized using an opto-electronics
90 station built and calibrated at Argonne National Laboratory [11]. Figure 2 (b) shows the typical
91 photocathode QE values as a function of incident light wavelength. The peak QE value is ~23% at 370 nm,
92 with the quick drop at short wavelength due to the strong PMT glass absorption in that range. Current-
93 voltage (I-V) curve was also measured with a stable beam at 370 nm. As the bias voltage increased, the
94 photocurrent increased, indicating that more and more photoelectrons were collected until it reached a
95 maximum value, indicating the maximum photoelectron collection yield was reached.

96



97

98

99

100

101

102 3. Design of glass vessel for large area planar photocathode deposition

103

104

105

106

107

108

109

110

111

112

113

114

Figure 2. (a) 1-inch diameter photocathode deposited in a PMT glass vessel. (b) Typical QE curve of K-Cs-Sb bi-alkali PMT photocathode in the range 300-600 nm. Inset: I-V curve of the photocathode. The data were measured in the setup described in ref. [11].

The compact geometry of large area MCP-based planar photodetector does not have space to contain the evaporation sources inside the detector package, which requires a transfer photocathode process rather than the in-tube process described in section 2. The photocathode was first deposited on a glass plate and then the glass plate was transferred under vacuum into a sealing chamber, where a tile containing pre-prepared microchannel plates and electronic feedthroughs were ready for final packaging. This transfer process also avoids the destructive contamination from alkali vapors (K, Cs) of the microchannel plates during photocathode deposition process.

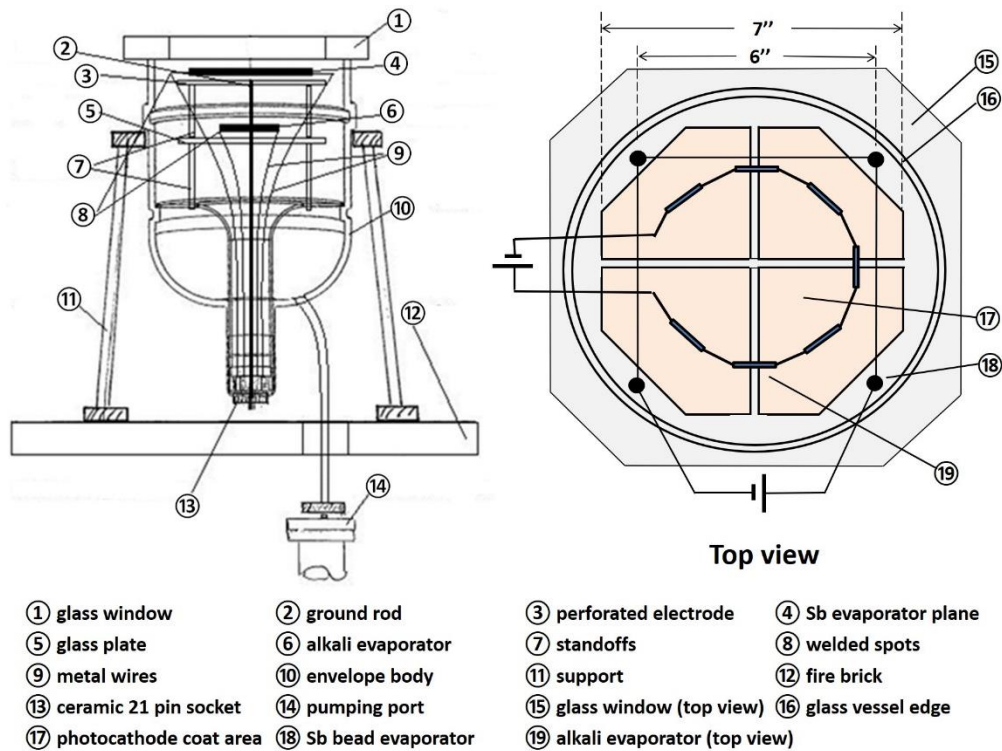
To demonstrate the feasibility of scaling up the photocathode growth recipe employed in small PMT tube to large area photocathode, we designed and built a large glass vessel based on the conventional PMT glass vessel, as shown in Figure 3. The size of the glass vessel was designed to fit in the bakeout oven and to be compatible with the existing vacuum system as mentioned in Section 2. The glass vessel was a tube-shaped

115 body and a replaceable top window with active photocathode area as large as $\sim 41 \text{ inch}^2$. Inside the glass
116 vessel, the evaporation system was built in three levels similar to the small PMT tube design: antimony
117 beads which were closest to the window, alkali dispensers which were furthest from the window, and a
118 perforated electrode which was in between the antimony beads level and alkali dispensers level, used for
119 applying RF-power during plasma treatments and for collecting photoelectrons. With the large opening and
120 volume of the glass vessel, evaporator sources could be easily installed inside the vessel, and the amount,
121 geometry and contact mechanism of individual evaporator sources could be freely modified for process
122 optimization. At the bottom of the glass vessel, all electrical leads for source heating and measurements
123 were connected to the outside through a glass connector with 21-pin electrical feedthroughs. A vacuum port
124 near the bottom connects the vessel to a high vacuum pump, and base pressure at 10^{-7} Torr level was
125 achieved after overnight baking.

126

127 To evaluate the QE uniformity of the large, planar photocathode, an X-Y scanner was installed outside on
128 top of the glass vessel. Collimated beam from a movable QE measurement system [11] was introduced to
129 the scanner through an optical path for *in-situ* measurement and QE distribution scanning.

130



131

132

Figure 3. Schematic of custom designed glass vessel for large area planar photocathode demonstration and

133

recipe development; the right figure shows the top view of the vessel for evaporator configuration and

134

position illustration, which may affect the QE distribution pattern.

135

136 4. Large area uniform planar photocathode

137 4.1 Photoemission process

138

In many experiments, the most important property of a PMT of interest is its QE, i.e., the fraction of photons

139

converted into photoelectrons as a function of wavelength. In PMT applications, most of the photocathodes

140

are of transmission mode, i.e, semitransparent films. When incident light reaches a PMT, part of the light

141

is absorbed by the photocathode, the other parts are either reflected or transmitted through the PMT window

142

and photocathode. The photons that are absorbed by the photocathode contribute to the production of

143

photoelectrons through the photoelectric effect. Classically, the photoemission process is described by the

144

simplified Three-Step model [12]: (1) the photoexcitation of the electrons; (2) transport to the surface; (3)

145 escape from the material surface to vacuum. Considering the three-step process, the quantum efficiency can
146 be expressed below as a product of two probabilities conveniently [13, 14]:

$$147 \quad QE(\lambda) = A(\lambda) \times P_{conv}(\lambda) \quad (1)$$

148 where $A(\lambda)$ is the probability of photons being absorbed by the photocathode where it is dependent upon
149 the refractive indices of the material and the PMT optical geometry design, and $P_{conv}(\lambda)$ is the probability
150 of such absorption to produce photoelectrons through photoemission process, which in turn depends on the
151 photoelectron escape length (L) and photocathode work function (ϕ).

152

153 Examining the photoemission process, it is realized that the thickness of the transmission mode
154 photocathode should have a critical optimum value. If the photocathode is too thin, most of the incident
155 light is transmitted rather than absorbed, yielding low QE. On the other hand, if the photocathode is too
156 thick, exceeding the escape length of the photoelectrons, the photoelectrons produced by absorbed light
157 cannot escape into the vacuum, also yielding low QE. Thus, it is necessary to deposit the photocathode with
158 optimum thickness for highest photoelectron emission and best spectral response. The optimum
159 photocathode thickness represents the compromise between the light transmission loss and the electron
160 scattering loss. Here, we must emphasize that the optimum thickness of semitransparent photocathode is
161 not a unique number along the whole spectrum. It has different values for different response wavelength as
162 the material absorption coefficient and electron escape length are both wavelength dependent. For our
163 experiment and applications, the QE and thickness study were limited to the single wavelength $\lambda = 370$ nm,
164 which is the peak wavelength of K-Cs-Sb photo response.

165

166 **4.2 Correlation between photocathode performance and initial antimony layer thickness**

167 The bialkali K-Cs-Sb photocathode in PMT is a thin layer of semiconductor deposited at the back side of
168 the glass window, and it is not chemically stable when exposed to air. This makes it difficult to directly
169 measure the photocathode thickness using *ex-situ* thin film characterization methods and to find the
170 optimum thickness. Nevertheless, several studies on the K-Cs-Sb cathode chemical composition and

171 structure [15, 16] showed that the photocathode is a compound with stoichiometric formula near K_2CsSb .
172 Reviewing the sequential photocathode growth process in Section 2, the whole process can be expressed
173 by the following chemical process:

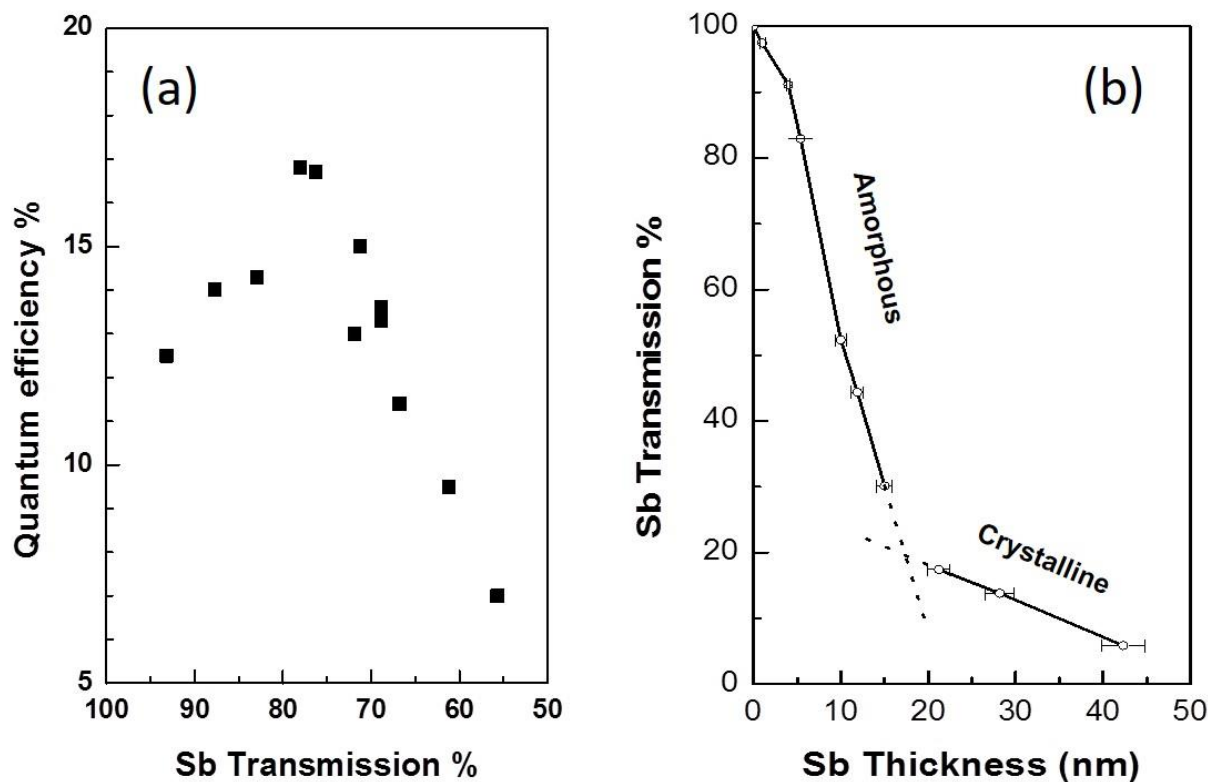


175 The K_2CsSb photocathode thickness is predominantly dictated by the initial Sb film thickness, thus the
176 initial Sb film should also have an optimum thickness for best photocathode performance.

177
178 The custom-designed large glass photocathode deposition vessel provides us an ideal facility to study the
179 effect of initial antimony film thickness on the overall photocathode performance. With the large flat glass
180 window, we were able to mask the area and deposit Sb film with gradient thickness. The QE distribution
181 of the subsequently fabricated photocathode is thus related to the initial Sb film thickness distribution. A
182 common and practical way to measure the relative thickness of a metal thin film on transparent substrate is
183 optical methods such as reflection and transmission. With the laser beam normal to the substrate surface,
184 the transmission measurement is much easier to set up than the reflectance, thus we focused our
185 measurement using the transmitted light.

186
187 We measured the light transmission distribution of the Sb film at $\lambda = 370$ nm across the glass plate before
188 photocathode growth, and the QE distribution of the large area photocathode after deposition. The Sb film
189 transmission was defined as the ratio of light intensity across the glass plate with and without Sb deposition.
190 The incident light direction is normal to the surface of the glass plate. The correlation between QE and Sb
191 film transmission is plotted in Figure 4 (a). It is clear from the curve that the highest QE for K_2CsSb
192 photocathode is fabricated from Sb film with transmission around 75%. This value is similar to the reported
193 optimum Sb film transmission around 82% for Cs_3Sb photocathode [17]. The decrease of QE at high Sb
194 transmission is due to the poor photon absorption in thin photocathode film, while the decrease of QE at
195 low Sb transmission is due to the poor photoelectron escape in thick photocathode film.

196



197

198

199 Figure 4. (a) Quantum efficiency vs. initial antimony film transmission. The highest QE photocathode was
 200 obtained from Sb film with ~75% transmission (~7nm). Data error bars are not shown as they are smaller
 201 than the size of the data points. (b) Sb film transmission vs. Sb film thickness, amorphous to crystalline phase
 202 transition occurs at ~20% transmission (~17 nm).

203

204 The transmission method is a relative measurement of Sb film thickness. It is of interest and necessary to
 205 investigate the dependence of transmission on absolute film thickness. A series of Sb films with thicknesses
 206 ranging 1 to 45 nm were deposited on masked glass with small area. The sample thickness was monitored
 207 by pre-calibrated quartz crystal microbalance (QCM) and further measured using X-ray reflectivity (XRR)
 208 and atomic force microscope (AFM). The results of the transmission vs. Sb film thickness are shown in
 209 Figure 4(b). The figure consists of two sections, breaking apart at about 30% transmission. It is well-known
 210 that the antimony growth performs a phase transition between amorphous and crystalline structure. The

211 change of transmission trend at 20% ~ 30% is an indication of the phase transition in Sb film. The critical
212 phase transition thickness is around 17 nm for Sb deposited on glass, agreeing with the reported thickness
213 (9~12 nm) [18]. The slightly higher transition thicknesses here than the reported thickness may due to the
214 different growth conditions: temperature, vacuum level, growth rate etc. The optimum Sb thickness for
215 K₂CsSb photocathode fabrication is ~7 nm, and it is an amorphous film.

216

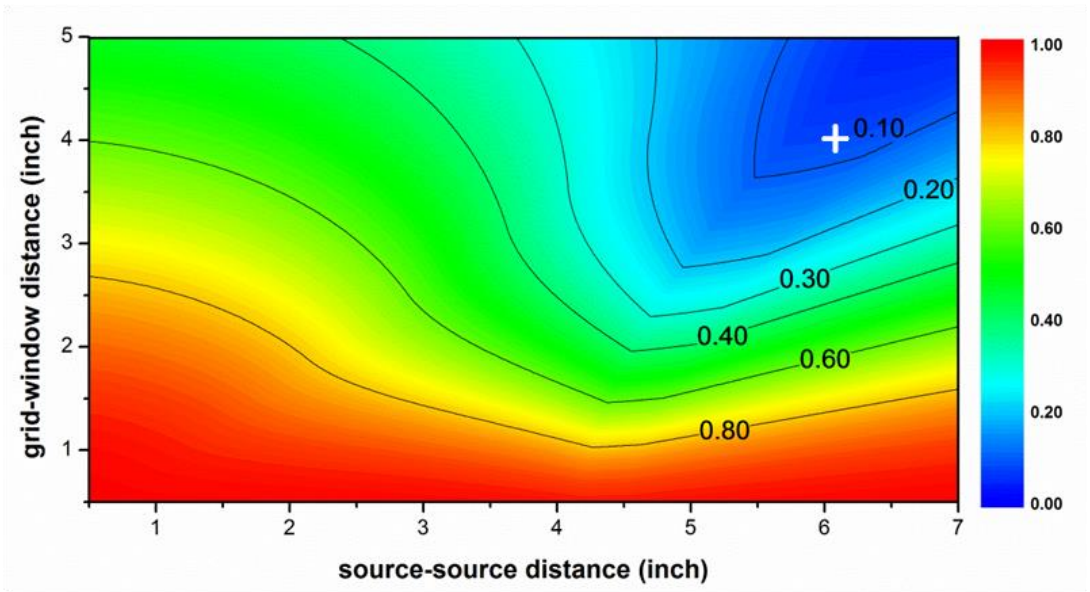
217 **4.3 Antimony film uniformity simulation**

218 For a large area planar photodetector, the uniformity of photocathode is one important factor for accurate
219 data measurement. As stated earlier, the Sb film thickness distribution affects the overall photocathode
220 quantum efficiency distribution. It is important to produce antimony film with constant and controlled
221 thickness for uniform photocathode. Obviously, the further the source is placed away from the glass window,
222 the better the film uniformity can be achieved. However, this could make the glass vessel impractically
223 large and requires a large Sb source to be able to achieve the necessary thickness. To reduce the source and
224 window space and achieve uniform Sb film with thickness variation less than 10%, we used multiple Sb
225 sources configuration and investigated the optimum placement of these sources via a simulation of the
226 evaporation thickness. As stated earlier, the point-like Sb beads were placed on a square grid parallel to the
227 flat glass window (Figure 3). The following assumptions were made: (1) each bead evaporates identically,
228 (2) antimony atoms travel in straight lines to the window, (3) the sticking coefficient does not depend on
229 the incidence angle. Thus, the deposited thickness is solely related to the distance between the deposition
230 location and location of each bead, i.e.:

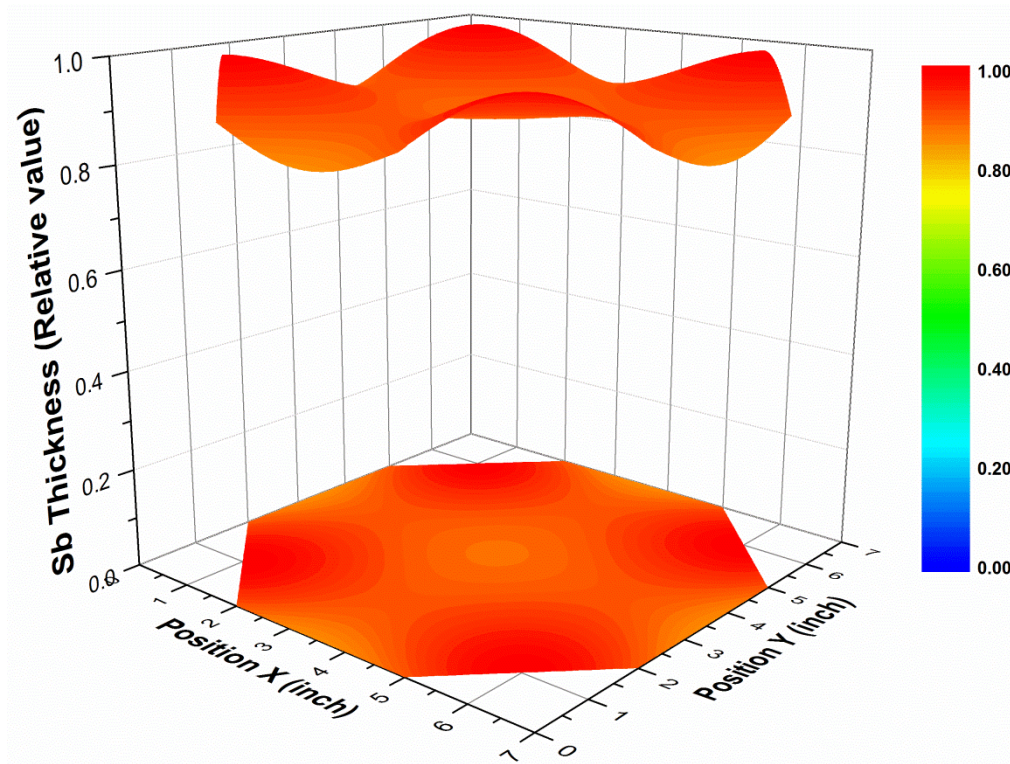
$$231 \quad t \propto \sum \frac{1}{r_i^2} \quad (3)$$

232 where t is the deposition thickness and r_i is the evaporation distance, i.e. the distance between deposition
233 area and the i th bead. The evaporation distance is geometrically related to the source grid to window
234 distance and the source to source distance, which are both limited by the vessel size. Here, we fixed the
235 number of beads to be 4, and simulated the thickness variation dependence of the space distance and

236 separation distance, the result is shown in Figure 5. The thickness variation reduces as the space distance
237 and separation distance increases given the fixed bead number. The upper right area indicates the preferred
238 configuration for a uniform film deposition. Limited by the glass vessel size, a configuration of 4 inches
239 space distance and 6 inches separation distance (indicated in Figure 5) was chosen for both numerical and
240 experimental studies. Figure 6 shows the simulated uniformity for the optimal configuration of four
241 antimony beads. The simulated Sb thickness variation for a masked 7 inches \times 7 inches area (with activation
242 area of ~ 40 inch²) is below 10%.
243



244
245
246 Figure 5. Simulation of the Sb film thickness variation dependence on the grid-window distance and source
247 separation distance. The color scale and values indicate the thickness variation of the film with the Sb source
248 at the according x-y configuration. The upper right corner is the preferred configuration, and “+” indicates
249 the chosen configuration for our experiment, with thickness variation of 10%.
250



251

252

253 Figure 6. Simulated Sb film thickness distribution with four Sb bead sources 6 inches apart on a square grid,
 254 the distance between Sb sources and top window is 4 inches for a uniform thickness variation below 10%.

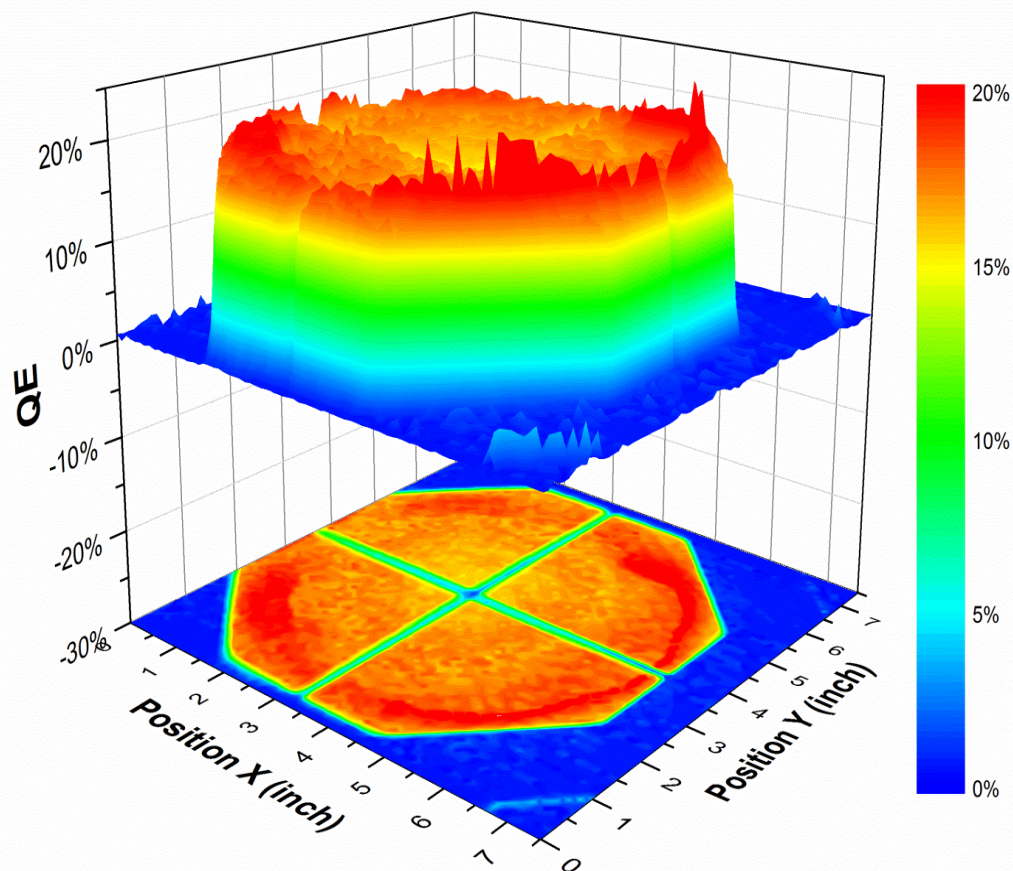
255

256 4.4 Large area uniform planar photocathode fabrication

257 Planar photocathodes with large activation area were fabricated in the custom-designed glass vessel by
 258 adopting the sequential recipe described in Section 2. The recipe was further modified based on the
 259 experiment and simulation to achieve the best uniformity. Four Sb/Pt sources were placed in a square
 260 configuration with source-to-source side length 6 inches on a grid, which was 4 inches away from the flat
 261 glass window. Figure 7 shows the QE distribution of the 40 inch² masked photocathode. The edges and the
 262 cross lines at the center are the aluminum mask, serving as the electronic connection from photocathode
 263 inside the vacuum to outside connectors in air. The QE of the planar photocathode was 18% with standard
 264 deviation (σ) of 1% over the 40 inch² activation area.

265

266 Comparing Figure 6 with Figure 7, we noticed that the QE distribution exhibits a high QE concentric pattern
267 along the edge area, which is different from the simulated Sb film thickness distribution pattern. This
268 concentric QE distribution pattern is most likely due to the configuration geometry of alkali dispensers,
269 which were placed as a circle as shown in Figure 3. Due to the large volume of the glass vessel, multiple K
270 dispensers were connected in series to ensure there were sufficient K during the photocathode growth.
271 Multiple Cs dispensers were also connected in series in case of Cs shortage. The circle geometry of alkali
272 dispensers may provide alkali vapor concentration gradient during photocathode growth, resulting in a
273 concentric QE distribution at the edge. A careful re-configuration of the alkali dispenser positions to achieve
274 uniform alkali vapor concentration will be considered in future photocathode growth. The grown
275 photocathode exhibits an average QE value of 18%, and maximum QE value of 20%, which is slightly
276 lower than that of the PMT tube photocathode (23%). There may be two main reasons for the lower QE:
277 (1) the Sb film in the central region may be not fully reacted, a better configuration of alkali dispensers in
278 central region or extension of alkali vapor coating time should be implemented to allow complete reaction
279 for enhanced QE value; (2) the antireflection layer was omitted during this planar photocathode fabrication
280 due to the difficulty with plasma ignition to form the antireflective film in the glass vessel, improvement
281 on the antireflection layer design and optimization based on optical principle is also expected to further
282 enhance the large area photocathode QE.



283

284 Figure 7. QE distribution of a masked photocathode with 40 inch² sensitive area at 370 nm (QE measurement
 285 was made in a current mode). The edge area and the cross lines are Al-coated mask, serving as electrical
 286 connection between photocathode and electrical feedthrough pins. The minute QE response on the cross lines
 287 is due to that the light spot is larger than the line.

288

289 5. Conclusion

290 A large glass vessel was designed and built for large area planar bi-alkali photocathode demonstration. The
 291 sequential photocathode process was investigated, and the optimum initial Sb film thickness was
 292 determined to be ~7 nm. The Sb source arrangement and configuration were optimized through numerical
 293 simulation for better Sb film thickness uniformity. Planar photocathodes with large area were fabricated in
 294 the custom-designed glass vessel with modified sequential process based on the experiment and simulation.
 295 We demonstrated the fabrication of bi-alkali photocathode with average QE of 18% at ~ 40 inch² activation

296 area for MCP-based photodetectors. The QE value and uniformity were further discussed to provide
297 possible improvements to enhance the performance of the photocathode in future.

298

299 **6. Acknowledge**

300 The authors wish to acknowledge the great assistance from P. Hink, Y. Li, R. Hosier, and J. DeFazio from
301 Photonis, USA. We would like to thank H. Frisch, K. Byrum and all the collaborators on the LAPPD project
302 for their valuable guidance. We would also like to thank J. Gregar and R. Northrop for their excellent work
303 on making the glass photocathode deposition vessel. We gratefully acknowledge an anonymous reviewer
304 whose insightful comments helped improve and clarify this manuscript. Work at Argonne National
305 Laboratory was supported by the U. S. Department of Energy, Office of Science, Office of High Energy
306 Physics under contract DE-AC02-06CH11357. Use of the Center for Nanoscale Materials was supported
307 by the U. S. Department of Energy, Office of Science, Office of Basic Energy Sciences, under Contract No.
308 DE-AC02-06CH11357.

309

310 **REFERENCES**

- 311 [1] A. G. Wright, *The Photomultiplier Handbook*, Oxford University Press, 1st edition (2017).
- 312 [2] S. Fukuda, *et al.*, “The Super-Kamiokande detector”, *Nucl. Instr. and Meth. A* **501**, 418 (2003).
- 313 [3] K. Abe, *et al.*, “Hyper-Kamiokande Design Report”, (2018). arXiv:1805.04163
- 314 [4] Z. Wang, “JUNO Central Detector and its prototyping”, *J. Phys.: Conf. Ser.* **718**, 062075 (2016).
- 315 [5] C. Adams, *et al.*, “The Long-Baseline Neutrino Experiment: Exploring Fundamental Symmetries of the Universe”,
316 (2013). arXiv:1307.7335
- 317 [6] I. Anghel, *et al.*, “Letter of Intent: The Accelerator Neutrino Neutron Interaction Experiment (ANNIE)”, (2015).
318 arXiv:1504.01480
- 319 [7] A. U. Mane, *et al.*, “An Atomic Layer Deposition Method to Fabricate Economical and Robust Large Area
320 Microchannel Plates for Photodetectors”, *Physics Procedia* **37**, 722 (2012).
- 321 [8] D. Kotchetkov, *et al.*, “Front-end electronic readout system for the Belle II imaging Time-Of-Propagation
322 detector”, *Nucl. Instr. and Meth. A* **941**, 162342 (2019).

- 323 [9] B. Adams, *et al.*, “A brief technical history of the Large-Area Picosecond Photodetector (LAPPD) Collaboration”,
324 (2016). arXiv:1603.01843
- 325 [10] A.H. Sommer, “A new alkali antimonide photoemitter with high sensitivity to visible light”, *Appl. Phys. Lett.* **3**,
326 62 (1963).
- 327 [11] Junqi Xie, Klaus Attenkofer, Marcel Demarteau, Henry Frisch, Seon Lee, Alexander Paramonov, Robert Wagner,
328 and Zikri Yusof, “Instrumentation for Theory-Inspired Photocathode Development within the Large Area
329 Picosecond Photodetector (LAPPD) Project”, *Physics Procedia* **37**, 811 (2012).
- 330 [12] W. E. Spicer, “Photoemissive, photoconductive, and optical absorption studies of alkali-antimony compounds”,
331 *Phys. Rev.* **112**, 114 (1958).
- 332 [13] D. Motta, and S. Schonert, “Optical properties of bialkali photocathodes”, *Nucl. Instr. and Meth. A* **539**, 217
333 (2005).
- 334 [14] Kodai Matsuoka, “Expression for the angular dependence of the quantum efficiency of a thin multi-alkali
335 photocathode and its optical properties”, *Progress of Theoretical and Experimental Physics* **12**, 123H01 (2018).
- 336 [15] W. H. McCarroll, “Chemical and structural characteristics of the potassium-cesium-antimony photocathode”, *J.*
337 *Phys. Solids* **26**, 191 (1965).
- 338 [16] C. Ghosh, and B. P. Varma, “Preparation and study of properties of a few alkali antimonide photocathodes”, *J.*
339 *Appl. Phys.* **49**, 4549 (1978).
- 340 [17] M. Rome, “Relation of Antimony Transmission and the Photoelectric Yield of Cs-Sb”, *J. Appl. Phys.* **26**, 166
341 (1955).
- 342 [18] G. A. Condas, “Properties and Preparation of Thin Antimony Films of High Uniformity”, *Rev. Sci. Instrum.* **33**,
343 987 (1962).